IET Microwaves, Antennas & Propagation

Research Article

IET Journals
The Institution of Engineering and Technology

Input impedance and radiation pattern of a resonant dipole embedded in a two-dimensional periodic leaky-wave structure

ISSN 1751-8725
Received on 23rd February 2015
Accepted on 19th June 2015
doi: 10.1049/iet-map.2015.0324
www.ietdl.org

Ahmad Bakhtafrouz[1] ✉, *Amir Borji*[2]

[1]*Department of Electrical and Computer Engineering, Isfahan University of Technology, Isfahan 84156-83111, Iran*
[2]*Department of Electrical Engineering, Sharif University of Technology, Tehran 14588-89694, Iran*
✉ *E-mail: bakhtafrouz@ec.iut.ac.ir*

Abstract: Array scanning method (ASM) is employed to study the input impedance and radiation pattern of a two-dimensional periodic leaky-wave antenna (LWA). The antenna consists of a narrow horizontal strip dipole of arbitrary length underneath a two-dimensional (2D) periodic screen of metallic patches, which acts as a partially reflective surface (PRS), and backed by a ground plane. First, the Green's function in the presence of the 2D array of metallic patches is calculated by means of the ASM and then the current distribution and input impedance of the source dipole are calculated through the electric field integral equation and method of moments. The far-field pattern is computed using the reciprocity theorem. Compared to the Hertzian dipole, which is the only type of source that has been considered in the literature, the resonant dipole substantially improves the performance of periodic LWA in terms of radiated power, efficiency and bandwidth. Numerical results are given for a resonant dipole over the frequency range of 60–70 GHz and compared with those obtained from commercial softwares, FEKO® and Ansys HFSS®, showing an excellent agreement with considerable improvement in terms of memory usage and computational speed.

1 Introduction

Leaky-wave antennas (LWAs) are a class of travelling wave antennas capable of producing narrow beams that can be scanned with frequency [1]. The radiation mechanism of LWAs is based on the existence of a guided wave with complex propagation constant that loses energy to space waves as it travels along the structure. The phase constant controls the scan angle, while the attenuation constant controls the beamwidth [2]. Planar LWAs have attracted more attention because of their low profile, low cost, ease of fabrication and seamless integration with printed circuits.

From the geometry viewpoint, LWAs are divided into two types: non-periodic structures such as long slots on waveguide walls [1] and periodic structures such as periodic holes in a waveguide wall [1, 3] or periodically loaded planar transmission lines. Planar LWAs can also be classified as one-dimensional (1D) or two-dimensional (2D) structures. In 1D LWA a travelling wave with a constant direction radiates, while in 2D LWA a radial cylindrical wave leaks into space. Recently, 2D periodic LWAs have attracted considerable attention because of their capability to produce a pencil beam at broadside as well as a narrow conical beam at other angles [4–6].

Previous studies of 2D periodic LWAs such as [2, 4–7] and 2D uniform planar LWAs such as [8–10] have mainly focused on computing the far-field radiation pattern by proper application of reciprocity theorem. There is hardly any published data available on the input impedance except for a few experimental results [11]. Furthermore, in 2D periodic LWAs, the excitation is usually considered to be a Hertzian electric or magnetic dipole and resonant antennas have not been explored [2–6, 12].

In this paper, the input impedance as well as the radiation pattern of 2D periodic LWAs that are excited by a resonant dipole are investigated. A brute-force and time-consuming method to obtain the antenna characteristics is to solve a sufficiently large but finite problem which is obtained by truncating the infinite periodic structure after a sufficiently large number of periods. However, in this paper, a highly efficient technique is presented which takes advantage of periodicity of the medium in which the source dipole is embedded by employing the array scanning method (ASM) [12–15]. First, the Green's function of the periodic leaky-wave structure is found using the ASM. Next, the current distribution and input impedance of the dipole antenna are calculated and, finally, the far field pattern of the LWA is obtained by invoking the reciprocity theorem. The above steps involve different types of electric field integral equations (EFIEs) that are solved using the method of moments (MoM). Full-wave numerical analysis of 2D periodic LWAs has not been reported previously in literature. Even the brute-force method mentioned above has not been implemented although it can be carried out by commercial electromagnetic solvers and it will be used for verification of numerical results in this paper.

2 Formulation

The 2D periodic LWA consists of a 2D array of metallic rectangular patches, which acts as a partially reflective surface (PRS), printed on a grounded dielectric slab as shown in Fig. 1. The periods of printed patches are p_x and p_y along the x and y directions, respectively. Each patch has the width of w_p and the length of l_p. The height of substrate layer is h and its dielectric constant is ε_r. A narrow strip dipole with length of l_s and width of w_s located at the height of $z_s < h$ excites the leaky wave in the periodic structure. A small gap of width w_g exists between the two arms of the dipole on which a delta-gap voltage source is applied.

2.1 EFIE for the dipole

Assume $\boldsymbol{J}_s$ is the current distribution on the surface of the strip dipole. The boundary condition requires

$$-\hat{\boldsymbol{z}} \times \boldsymbol{E}^i\big|_S = \hat{\boldsymbol{z}} \times \boldsymbol{E}^s_D(\boldsymbol{J}_s)\big|_S + \hat{\boldsymbol{z}} \times \boldsymbol{E}^s_{PRS}(\boldsymbol{J}_s)\big|_S \tag{1}$$

in which S is the surface of the strip dipole and $\boldsymbol{E}^i$ is the electric field of the delta-gap voltage source. $\boldsymbol{E}^s_D$ is the scattered electric field from $\boldsymbol{J}_s$ in the absence of 2D array of metallic patches and $\boldsymbol{E}^s_{PRS}$ is the scattered field from the 2D array when excited by $\boldsymbol{J}_s$. Using the

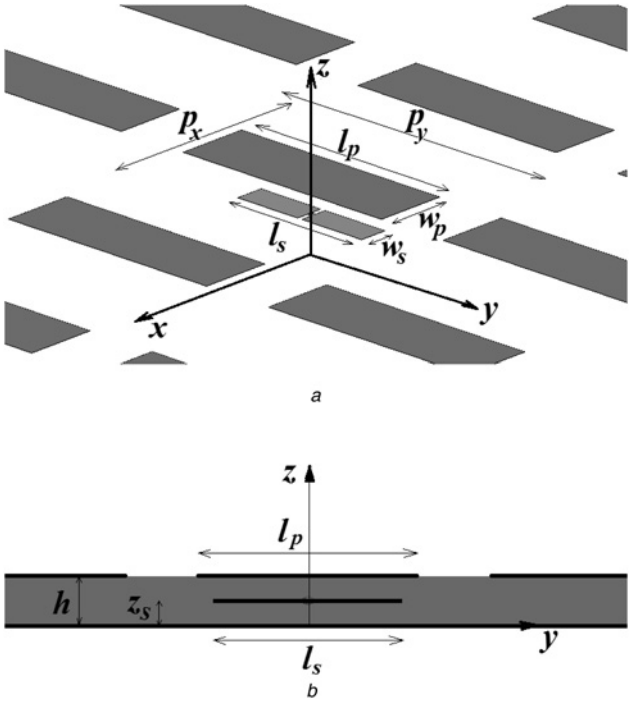

Fig. 1 *Periodic LWA structure excited by a strip dipole beneath the periodic array of patches. The ground plane at the back is not shown here. The strip dipole is excited by a delta-gap voltage source*

a 3D view
b Side view

appropriate Green's functions, the above equation can be written in the following form which presents an integral equation for $\boldsymbol{J}_s$

$$\boldsymbol{E}_D^s = -j\omega\overline{\overline{\boldsymbol{G}}}_A^d(x, y, z = z_s, x', y', z' = z_s) * \boldsymbol{J}_s - \nabla\left(K_\varphi^d(x, y, z = z_s, x', y', z' = z_s) * \nabla \cdot \boldsymbol{J}_s\right) \quad (2)$$

$$\boldsymbol{E}_{PRS}^s = \overline{\overline{\boldsymbol{G}}}_{EJ}^{PRS}(x, y, z = z_s,\ x', y', z' = z_s) * \boldsymbol{J}_s \quad (3)$$

in which the asterisk is a shorthand notation for surface convolution integral:

$$\overline{\overline{\boldsymbol{G}}} * \boldsymbol{J} = \int_{S'} \overline{\overline{\boldsymbol{G}}}(\boldsymbol{r}, \boldsymbol{r}') \cdot \boldsymbol{J}(\boldsymbol{r}')\, dS' \quad (4)$$

$\overline{\overline{\boldsymbol{G}}}_A^d$ and K_φ^d are the vector magnetic potential and scalar electric potential Green's functions of the grounded dielectric substrate in the absence of the periodic screen as shown in Fig. 2. $\overline{\overline{\boldsymbol{G}}}_{EJ}^{PRS}$ is the dyadic Green's function of the electric field in the presence of the 2D array of patches which is basically equal to the electric field that is caused only by the induced currents on the 2D array when excited by a Hertzian dipole located at (x', y', z_s) as shown in Fig. 3. Note that $\overline{\overline{\boldsymbol{G}}}_{EJ}^{PRS}$ does not include the electric field of the Hertzian dipole itself which is represented by the first term on the right-hand side of (1).

To solve (1) via the MoM, $\boldsymbol{J}_s$ is expanded by triangular Rao-Wilton-Glisson (RWG) basis functions [16]

$$\boldsymbol{J}_s(\boldsymbol{r}') = \sum_{n=1}^{N} I_n \boldsymbol{f}_n(\boldsymbol{r}') \quad (5)$$

where I_n are the unknown coefficients and $\boldsymbol{f}_n$ are the RWG basis functions which are defined on pairs of triangular subdomains [16]. Since all induced currents in this problem are horizontal, only $G_A^{d,xx}$ component of $\overline{\overline{\boldsymbol{G}}}_A^d$, which is equal to $G_A^{d,yy}$, and $G_{EJ}^{PRS,xx}$, $G_{EJ}^{PRS,xy}$, $G_{EJ}^{PRS,yx}$ and $G_{EJ}^{PRS,yy}$ components of $\overline{\overline{\boldsymbol{G}}}_{EJ}^{PRS}$ are needed. Using the Galerkin procedure for testing the integral equation, the following matrix equation is obtained

$$[\boldsymbol{Z}]_{N\times N}[\boldsymbol{I}]_N = [\boldsymbol{E}]_N \quad (6)$$

$$\begin{aligned} Z_{mn} = {} & j\omega \int\int_{S_m S_n} G_A^d(\boldsymbol{r}, \boldsymbol{r}')\boldsymbol{f}_m(\boldsymbol{r}) \cdot \boldsymbol{f}_n(\boldsymbol{r}')\, dS'\, dS \\ & - \int_{S_m} \nabla \cdot \boldsymbol{f}_m(\boldsymbol{r}) \int_{S_n} K_\varphi^d(\boldsymbol{r}, \boldsymbol{r}')\nabla' \cdot \boldsymbol{f}_n(\boldsymbol{r}')\, dS'\, dS \\ & - \int_{S_m}\int_{S_n} \boldsymbol{f}_m(\boldsymbol{r}) \cdot \overline{\overline{\boldsymbol{G}}}_{EJ}^{PRS}(\boldsymbol{r}, \boldsymbol{r}') \cdot \boldsymbol{f}_n(\boldsymbol{r}')\, dS'\, dS \end{aligned} \quad (7)$$

$$E_m = \int_{S_m} \boldsymbol{E}^i(\boldsymbol{r}) \cdot \boldsymbol{f}_m(\boldsymbol{r})\, dS \quad (8)$$

in which $G_A^d \triangleq G_A^{d,xx}$ and S_m is the domain of mth basis function. The kernels of the above integrals for $m = n$ are singular and must be treated with care. This singularity is extracted and analytically integrated by formulas given in [17] and then added back to the remaining regular part.

After solving (6), the input impedance of the dipole antenna is calculated by dividing the source voltage, which is assumed to be 1 V, by the total current passing through the width of the dipole at the location of the delta gap source.

2.2 Green's functions of the grounded dielectric slab without the periodic screen

As mentioned before, G_A^d and K_φ^d are the Green's functions for the magnetic vector potential and the scalar electric potential of a grounded dielectric slab in the absence of periodic array as shown in Fig. 2. Spatial forms of these Green's functions are usually derived by inverse Fourier transforms of their spectral domain representations which is finally written in the form of Sommerfeld integrals [18]. The integrand of Sommerfeld integrals always suffers from slow decay and oscillatory behaviour and various techniques have been proposed in the literature for efficient computation of these integrals [18–20]. However, in this paper, we propose an alternative method based on the ASM instead of Sommerfeld integrals to compute the spatial forms of G_A^d and K_φ^d which can be easily extended to an arbitrary multilayer structure.

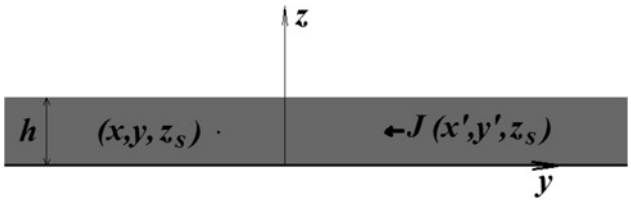

Fig. 2 *Structure for calculation of $\overline{\overline{\boldsymbol{G}}}_A^d$ and K_φ^d. The Hertzian dipole is in (x', y', z_s) and observation point is at (x, y, z_s)*

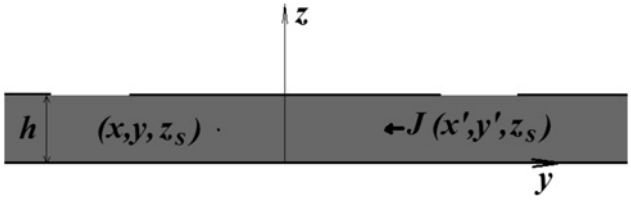

Fig. 3 *Structure for calculation of $\overline{\overline{\boldsymbol{G}}}_{EJ}^{PRS}$. The Hertzian dipole that excites the 2D array of patches is at (x', y', z_s) and the observation point is at (x, y, z_s)*

ASM is basically an analytical method to synthesise the field of an aperiodic source (such as a single-point source) from spectral integration of the field of an infinite phased array of periodic sources. Employing the concept of ASM, the current of a single dipole can be expressed by currents of a 2D phased array of dipoles [21]:

$$\boldsymbol{J}^{i,\mathrm{d}} = \frac{p_x p_y}{(2\pi)^2}\int_{-\pi/p_x}^{\pi/p_x}\int_{-\pi/p_y}^{\pi/p_y} \boldsymbol{J}^{i,PA}\left(k_x, k_y\right)\mathrm{d}k_x\,\mathrm{d}k_y \tag{9}$$

$\boldsymbol{J}^{i,\mathrm{d}}$ represents a single-point source at (x', y', z'), while $\boldsymbol{J}^{i,\mathrm{PA}}$ represents an infinite phased array of sources located at $(x' + mp_x, y' + np_y, z')$ with $m, n = 0, \pm 1, \pm 2, \ldots$ as shown in Fig. 4. k_x and k_y are the phase shifts between adjacent elements along x and y directions, respectively. Using (9) and linearity of Maxwell's equations, the Green's function of a single-point source can be expressed by a spectral superposition of the corresponding Green's function of infinite phased arrays with varying phase shifts

$$G_A^{\mathrm{d}}(\boldsymbol{r}, \boldsymbol{r}') = \frac{p_x p_y}{(2\pi)^2}\int_{-\pi/p_x}^{\pi/p_x}\int_{-\pi/p_y}^{\pi/p_y} G_A^{\mathrm{PA}}\left(\boldsymbol{r}, \boldsymbol{r}', k_x, k_y\right)\mathrm{d}k_x\,\mathrm{d}k_y \tag{10}$$

On the other hand, the Green's function of a 2D periodic structure is given by [22]

$$G_A^{\mathrm{PA}}\left(\boldsymbol{r}, \boldsymbol{r}', k_x, k_y\right) = \sum_{m=-\infty}^{\infty}\sum_{n=-\infty}^{\infty}\tilde{G}_A^{\mathrm{PA}}\left(k_{\rho,mn}, z, z'\right) \times \mathrm{e}^{-\mathrm{j}k_{xm}(x-x')}\,\mathrm{e}^{-\mathrm{j}k_{yn}(y-y')} \tag{11}$$

in which $k_{xm} = k_x + 2m\pi/p_x$, $k_{yn} = k_y + 2n\pi/p_y$ and $k_{\rho,mn} = \sqrt{k_{xm}^2 + k_{yn}^2}$. The spectral quantity $\tilde{G}_A^{\mathrm{PA}}$ can be found in closed form using the equivalent transverse transmission line model [23]. Similar equations also hold for K_φ^{d}.

The double series in (11) converges very slowly when $z = z'$. A very efficient method to calculate this series is to extract the asymptotic part of $\tilde{G}_A^{\mathrm{PA}}\left(k_{\rho,mn}, z, z'\right)$ for large m, n and then add it back in the form of Ewald summation [22]. We may call this technique Kummer decomposition-Ewald method. Moreover, for further improvement of computational efficiency, G_A^{d} and K_φ^{d} are computed and saved at discrete points of a uniform grid and then interpolated using spline method to find their values at other observation points [24]. Note that only a 2D interpolation based on variables $\Delta x = x - x'$ and $\Delta y = y - y'$ is sufficient.

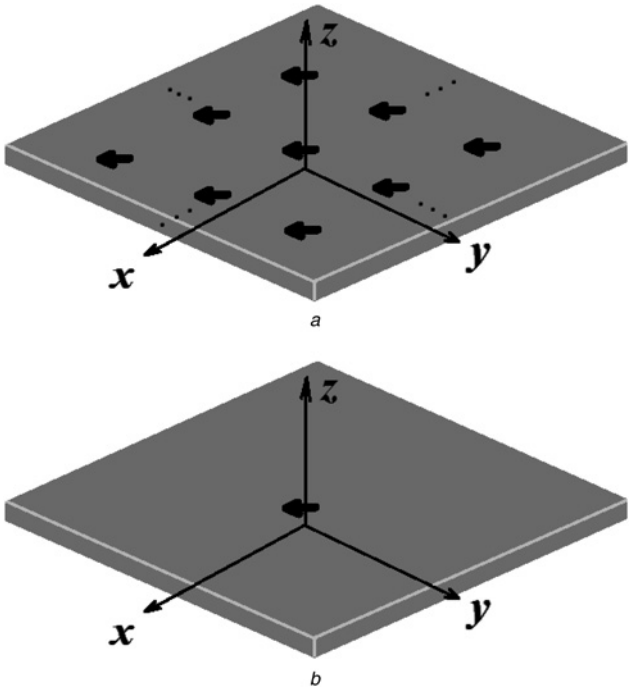

Fig. 4 *Current distributions in ASM integral*

a $\boldsymbol{J}^{i,\mathrm{PA}}$ is an infinite phased array of point sources located at $(x' + mp_x, y' + np_y, z')$
b $\boldsymbol{J}^{i,\mathrm{d}}$ is a single source at (x', y', z')

2.3 Calculation of the dyadic Green's function of the periodic screen

As explained in Section 2.1, $\bar{\bar{\boldsymbol{G}}}_{EJ}^{\mathrm{PRS}} \cdot \hat{\boldsymbol{J}}$ is the electric field that is caused only by the induced currents on the 2D array of patches when excited by a $\hat{\boldsymbol{J}}$-directed Hertzian dipole located at (x', y', z_s) and does not include the electric field of the Hertzian dipole itself. Again we use a method based on ASM, similar to the one presented in Section 2.2, to find the necessary components of $\bar{\bar{\boldsymbol{G}}}_{EJ}^{\mathrm{PRS}}$ numerically. Assume a phased array of x-directed dipoles is placed on $z' = z_s$ plane with the same periods of p_x and p_y. The following expression can be written based the concept of ASM

$$G_{EJ}^{\mathrm{PRS},xx}(\boldsymbol{r}, \boldsymbol{r}') = \frac{p_x p_y}{(2\pi)^2} \int_{-\pi/p_x}^{\pi/p_x}\int_{-\pi/p_y}^{\pi/p_y} G_{EJ}^{\mathrm{PRS},xx,\mathrm{PA}}\left(\boldsymbol{r}, \boldsymbol{r}', k_x, k_y\right)\mathrm{d}k_x\,\mathrm{d}k_y \tag{12}$$

$G_{EJ}^{\mathrm{PRS},xx,\mathrm{PA}}$ is the x component of the electric field that is caused by the induced currents on the 2D patch array (located on $z = h$ plane) when excited by a x-directed phased array of dipoles (located on $z = z_s$ plane) excluding the electric field of the phased array itself. Since this problem is a periodic one, we only need to find the induced current on the patch in one unit cell. This is accomplished by finding the induced current on the metallic patch through an EFIE and then calculating the electric field produced by this induced current using the well-known periodic Green's function. The EFIE for the single patch in the unit cell is obtained as follows

$$-\hat{\boldsymbol{z}} \times \boldsymbol{E}^{\mathrm{PA}}\big|_{\mathrm{patch}} = \hat{\boldsymbol{z}} \times \boldsymbol{E}^{\mathrm{PRS}}\big|_{\mathrm{patch}} \tag{13}$$

$$\boldsymbol{E}^{\mathrm{PA}} = -\mathrm{j}\omega\bar{\bar{\boldsymbol{G}}}_A^{\mathrm{PA}}(x, y, z = h, x', y', z' = z_s)\cdot\hat{\boldsymbol{J}} - \left(\nabla\nabla K_\varphi^{\mathrm{PA}}(x, y, z = h, x', y', z' = z_s)\right)\cdot\hat{\boldsymbol{J}} \tag{14}$$

$$\boldsymbol{E}^{\mathrm{PRS}} = -\mathrm{j}\omega\bar{\bar{\boldsymbol{G}}}_A^{\mathrm{PA}}\left(x, y, z = h,\ x', y', z' = h\right)*\boldsymbol{J}_{\mathrm{patch}} - \nabla\left(K_\varphi^{\mathrm{PA}}\left(x, y, z = h,\ x', y', z' = h\right)*\nabla\cdot\boldsymbol{J}_{\mathrm{patch}}\right) \tag{15}$$

Again, by expanding the induced current on the patch $\boldsymbol{J}_{\mathrm{patch}}$ with RWG basis functions and solving the EFIE of (13) via Galerkin method, the unknown coefficients of $\boldsymbol{J}_{\mathrm{patch}}$ are obtained. Now the electric field at (x, y, z_s) due to the induced currents on the 2D array can be calculated as follows

$$\boldsymbol{E}_{\mathrm{s}}^{\mathrm{PRS}} = -\mathrm{j}\omega\bar{\bar{\boldsymbol{G}}}_A^{\mathrm{PA}}\left(x, y, z = z_s,\ x', y', z' = h\right)*\boldsymbol{J}_{\mathrm{patch}} - \nabla\left(K_\varphi^{\mathrm{PA}}\left(x, y, z = z_s,\ x', y', z' = h\right)*\nabla\cdot\boldsymbol{J}_{\mathrm{patch}}\right) \tag{16}$$

If $\hat{\boldsymbol{J}} = \hat{\boldsymbol{x}}$ then

$$G_{EJ}^{\mathrm{PRS},xx,\mathrm{PA}} = E_{\mathrm{s},x}^{\mathrm{PRS}} \tag{17}$$

$$G_{EJ}^{\mathrm{PRS},yx,\mathrm{PA}} = E_{\mathrm{s},y}^{\mathrm{PRS}} \tag{18}$$

The above procedure must be repeated with a phase array of $\hat{y}$-directed dipoles to find $G_{EJ}^{\mathrm{PRS},xy,\mathrm{PA}}$ and $G_{EJ}^{\mathrm{PRS},yy,\mathrm{PA}}$. As can be seen

in (14)–(16), $\boldsymbol{G}_A^{\mathrm{PA}}$ and K_φ^{PA} for three different situations must be calculated through (11). Spectral domain Green's functions $\tilde{G}_A^{\mathrm{PA}}$ and $\tilde{K}_\varphi^{\mathrm{PA}}$ are given in Appendix I.

2.4 Far-field calculation

The reciprocity theorem can be employed to calculate the far-field pattern of the antenna. This method has been previously reported in [4] in connection with Hertzian dipole excitation of the periodic leaky-wave structure. A test dipole is placed at far zone of the antenna in $\hat{\boldsymbol{\theta}}$ ($\hat{\phi}$) direction to measure the radiated E_θ^{f} $\left(E_\varphi^{\mathrm{f}}\right)$. The $\hat{\boldsymbol{\theta}}$-directed ($\hat{\phi}$-directed) test dipole generates a TM (TE) polarised plane wave that illuminates the 2D periodic structure including the substrate and ground plane but in the absence of the strip dipole whose actual surface current density $\boldsymbol{J}_{\mathrm{s}}$ was calculated by solving the matrix equation of (6) in Section 2.1. Now from the reciprocity theorem, we can evaluate the radiated field of the LWA as follows

$$E_\theta^{\mathrm{f}}(r,\,\theta,\,\varphi) = \int_S \boldsymbol{E}_{\mathrm{tot}}^{\mathrm{d}}(x',\,y',\,z_{\mathrm{s}}) \cdot \boldsymbol{J}_{\mathrm{s}}\,\mathrm{d}x'\,\mathrm{d}y' \tag{19}$$

in which S is the surface of the strip dipole that launches the leaky wave. $\boldsymbol{E}_{\mathrm{tot}}^{\mathrm{d}}$ is the total electric field caused by the test dipole (located at far zone) calculated at the place of the strip dipole. Therefore, the problem is now reduced to a conventional plane-wave scattering from a 2D periodic structure on a grounded substrate. We can decompose $\boldsymbol{E}_{\mathrm{tot}}^{\mathrm{d}}$ into two components

$$\boldsymbol{E}_{\mathrm{tot}}^{\mathrm{d}} = \boldsymbol{E}_{\mathrm{sca}}^{\mathrm{sub}} + \boldsymbol{E}_{\mathrm{sca}}^{\mathrm{PA}} \tag{20}$$

where $\boldsymbol{E}_{\mathrm{sca}}^{\mathrm{sub}}$ is the electric field that is generated by the incoming plane wave in the absence of the 2D array and accounts only for the reflection from the grounded substrate and $\boldsymbol{E}_{\mathrm{sca}}^{\mathrm{PA}}$ is the electric field generated by the induced currents on the metallic patches due to the incoming plane wave. The incident field generated by the test dipole is a plane wave given by

$$\boldsymbol{E}_{\mathrm{inc}}^{\mathrm{d}}(\boldsymbol{r}') = \left(-\mathrm{j}\omega\mu_0 \frac{\mathrm{e}^{-\mathrm{j}k_0 r}}{4\pi r}\right) \mathrm{e}^{\mathrm{j}k_0 \hat{\boldsymbol{i}}\cdot\boldsymbol{r}'} \hat{\boldsymbol{\theta}} \tag{21}$$

with $\hat{\boldsymbol{i}} = \sin\theta\cos\varphi\hat{\boldsymbol{x}} + \sin\theta\sin\varphi\hat{\boldsymbol{y}} + \cos\theta\hat{\boldsymbol{z}}$ and $\boldsymbol{r}' = x'\hat{\boldsymbol{x}} + y'\hat{\boldsymbol{y}} + z'\hat{\boldsymbol{z}}$. Using the transverse equivalent transmission line, transverse components of $\boldsymbol{E}_{\mathrm{sca}}^{\mathrm{sub}}$ in (20) can be expressed as

$$\boldsymbol{E}_{\mathrm{sca,T}}^{\mathrm{sub}}\big|_{z'=z_s} = \boldsymbol{E}_{\mathrm{inc,T}}^{\mathrm{d}}\big|_{z'=h}\left(1+\Gamma_{\mathrm{TM}}\right)\frac{\sin(k_z z_{\mathrm{s}})}{\sin(k_z h)} \tag{22}$$

where the subscript $_{\mathrm{T}}$ denotes transverse components, Γ_{TM} is the reflection coefficient for TM plane wave at the top surface of the grounded dielectric substrate and k_z is defined by

$$k_z = k_0\sqrt{\varepsilon_r - \sin^2\theta} \tag{23}$$

$\boldsymbol{E}_{\mathrm{sca}}^{\mathrm{PA}}$ is found after calculating the induced currents on the metal patches in the presence of the grounded substrate. To find these induced currents, the following boundary condition is applied on the metallic patch in one unit cell of the periodic screen

$$-\boldsymbol{E}_{\mathrm{sca,T}}^{\mathrm{sub}}\big|_{\mathrm{patch}} = \boldsymbol{E}_{\mathrm{sca,T}}^{\mathrm{PA}}\big|_{\mathrm{patch}} \tag{24}$$

The left-hand side of (24) is given by (22) when z_{s} is replaced by h. The right-hand side of (24) is given by (15); however, this time $\boldsymbol{J}_{\mathrm{patch}}$ is the unknown induced current due to the incident plane wave. After solving the resulting EFIE with the MoM, $\boldsymbol{E}_{\mathrm{sca}}^{\mathrm{PA}}$ in (20) (at the location of strip dipole) can be calculated by (16).

3 Numerical results

In this section, numerical results are given for a narrow strip dipole with the length of $l_{\mathrm{s}} = 1.6$ mm and width of $w_{\mathrm{s}} = 0.2$ mm which is located in the middle of the dielectric layer at $z_{\mathrm{s}} = h/2$. The substrate permittivity is $\varepsilon_r = 2.2$ and other parameters are as follows: $l_{\mathrm{p}} = 2$ mm, $w_{\mathrm{p}} = 0.2$ mm, $p_x = 0.8$ mm and $p_y = 2.1$ mm. The required substrate thickness is selected based on the design equation given in [2]

$$\frac{h}{\lambda_0} = \frac{0.5}{\sqrt{\varepsilon_r - \sin^2\theta}} \tag{25}$$

which results in a substrate thickness of $h = 1.68$ mm in order to scan the beam from broadside to endfire in the frequency range of 60–81 GHz.

3.1 Input impedance

Figs. 5*a* and *b* show the input resistance (R_{in}) and reactance (X_{in}) of the antenna from 60 to 70 GHz, respectively. R_{in} and X_{in} were calculated for two different widths of the strip $w_{\mathrm{s}} = 0.2$, 0.4 mm whose corresponding antiresonance frequencies are $f_r = 63.02$, 61.38 GHz, respectively. To verify the calculations, a sufficiently large but truncated structure with 71×21 unit cells was simulated in FEKO which uses the surface integral equation method. Furthermore, a finite structure with 51×16 unit cells was simulated in HFSS which uses the finite element method and requires much more memory than FEKO. The simulated results are also shown in Figs. 5a and *b*. An excellent agreement can be seen between the proposed method and FEKO, while the presented

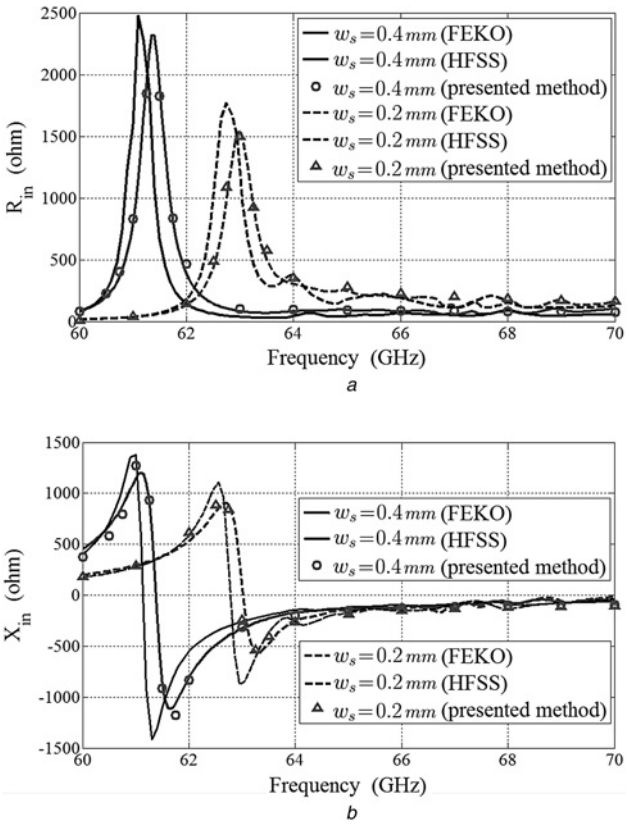

Fig. 5 *Input impedance of the strip dipole for two values of strip width when $z_s = h/2$ and $l_s = 1.6$ mm. FEKO and HFSS results are shown by lines and numerical results of the proposed method are shown by symbols*

a Resistance
b Reactance

IET Microw. Antennas Propag., 2015, Vol. 9, Iss. 14, pp. 1567–1573

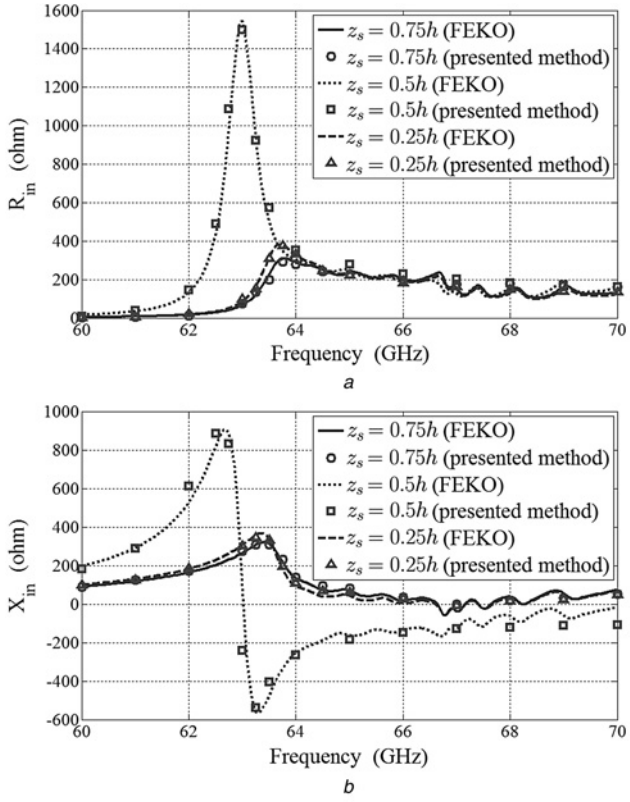

Fig. 6 *Input impedance of the strip dipole for three heights of the strip z_s. FEKO results are shown by lines, while numerical results of the proposed method are shown by symbols*

a Resistance
b Reactance

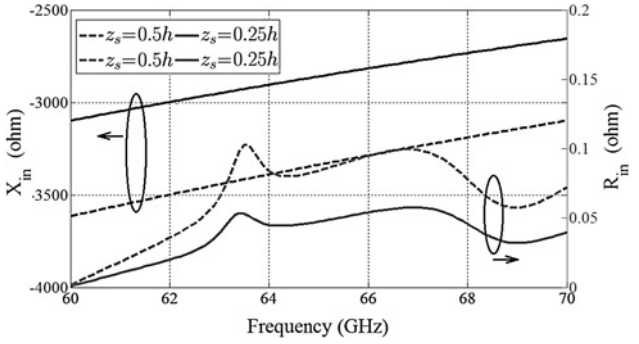

Fig. 7 *Input impedance of a very small dipole with $w_s = l_s = \lambda_{63}/100$ and $z_s = h/2$*

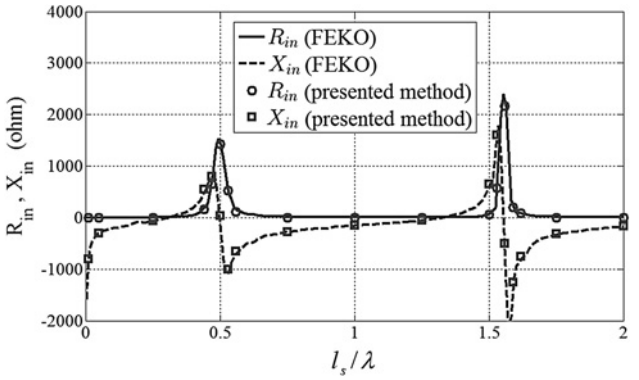

Fig. 8 *Input impedance of the strip dipole versus electrical length at 63 GHz with $w_s = 0.2$ mm and $z_s = h/2$. λ is the wavelength in the dielectric substrate at 63 GHz*

method is nine times faster than FEKO for an identical meshing of conductors and the same number of frequencies. A very good agreement is also seen with HFSS except for 0.4% frequency shift which is due to truncating the structure with smaller number of unit cells and different meshing.

The input resistance and reactance of the antenna for three different heights of the strip dipole, $z_s = h/4$, $h/2$, $3h/4$, are shown in Figs. 6*a* and *b*, respectively. Two interesting phenomena are observed in these plots: when the dipole is located at $z_s = h/2$ a sharp antiresonance occurs at $f_r = 63.02$ GHz where R_{in} is maximised and X_{in} crosses the zero axis with negative slope. The electrical length of the dipole at this frequency is $\lambda/2$ where λ is the wavelength in dielectric material. However, when the dipole is located at $z_s = h/4$ or $3h/4$, a clear-cut resonance does not occur but X_{in} remains close to zero over a wide bandwidth (65–70 GHz), while R_{in} remains close to 200 Ω. This property can be utilised to obtain a LWA which is fairly matched over a wide bandwidth, while its main beam is scanned. As far as the radiated power and efficiency are concerned, Fig. 6*a* shows that the best place for the source is $z_s = h/2$ where R_{in} can achieve a large value at 63 GHz albeit over a small bandwidth. In the following subsection, we will see that the antenna attains its narrowest beam at broadside at this antiresonance frequency. HFSS results were not included in Fig. 6 for better clarity because they showed an identical behaviour with only a slight deviation (almost 0.4%) in frequency.

To further appreciate the significance of exciting the LWA by a resonant dipole rather than a Hertzian dipole, the input impedance of a very small dipole with length of $\lambda_{63}/100$ was calculated and shown in Fig. 7. λ_{63} is the wavelength in the dielectric substrate at 63 GHz. This small dipole exhibits an extremely small resistance and a very large reactance over the entire bandwidth. Therefore, the radiated power would be very small compared to the resonant dipole and impedance matching would be extremely difficult and only possible over a narrow bandwidth.

Input impedance of the strip dipole versus its electrical length at 63 GHz is shown in Fig. 8. Here the wavelength is fixed at $\lambda = 3.21$ mm, which is the wavelength in the dielectric substrate at 63 GHz, while l_s changes from 0 to 6.4 mm. Two *parallel* resonances occur at $l_s = 0.5\lambda$ and 1.56λ, while there are two *series* resonances at $l_s = 0.31\lambda$ and 1.33λ where the input resistances are 11.5 and 5 Ω, respectively. For l_s =1.6 mm, if we remove the periodic screen from the top surface, the first anti-resonance occurs at 75.4 GHz with a much lower Q-factor, i.e. smaller reactance slope. Therefore, the periodic screen not only creates the leaky-wave mode, it also reduces the resonant length and bandwidth of the antenna. As we increase the width of the strip dipole, its resonant length decreases similar to a dipole antenna in homogeneous space. Fig. 9 shows the resonant length versus width of strip for the first antiresonance frequency.

Variation of resonant length versus frequency is rather interesting. Whereas in a homogeneous medium the electrical length of a dipole

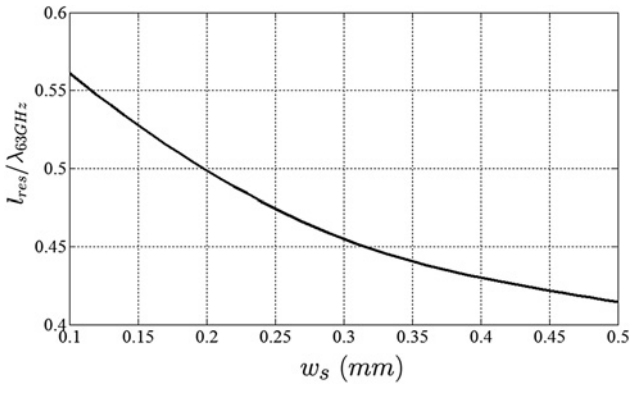

Fig. 9 *Resonant length versus width of strip dipole at 63 GHz for the first parallel resonance ($z_s = h/2$)*

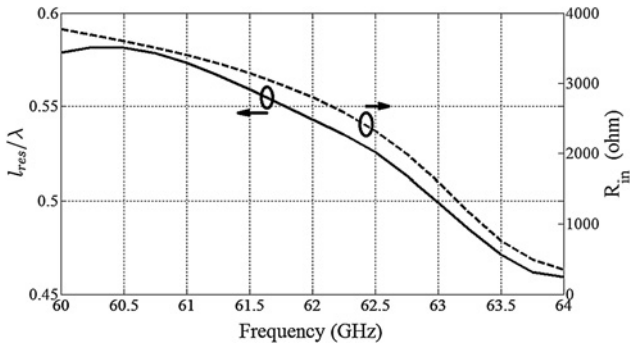

Fig. 10 *Resonant length and peak input resistance of the strip dipole vs. frequency for the first parallel resonance ($z_s = h/2$ and $w_s = 0.2$ mm)*

at resonance is independent of frequency (it remains equal to one wavelength for the first antiresonance), in this periodic structure if we increase the frequency from 60 GHz and sweep the dipole length at each frequency step, the electrical length at first antiresonance decreases as shown in Fig. 10. However, for frequencies above 63.5 GHz the first parallel resonance completely disappears and the reactance remains negative as we sweep the dipole's physical length. This is the frequency at which the main beam starts to split at broadside and two narrow beams start to appear which coincides with building up of reactive energy within the structure.

3.2 Radiation pattern

Radiation patterns of the antenna with $l_s = 1.6$ mm and $w_s = 0.2$ mm in H-plane ($\varphi = 0°$) and E-plane ($\varphi = 90°$) are shown in Figs. 11*a* and *b*, respectively. As the frequency increases from 60 to 63 GHz, the beam remains at broadside but the beamwidth decreases. Similar behaviour was reported in [4, 5] with a Hertzian dipole excitation. The beam scans away from broadside and splits into two narrow beams as frequency is increased further. Radiation patterns for scan angles of $\theta = 0°$, 15°, 30°, 45° were obtained at $f = 63$, 64, 66.35, 70 GHz, respectively. When compared to the results given

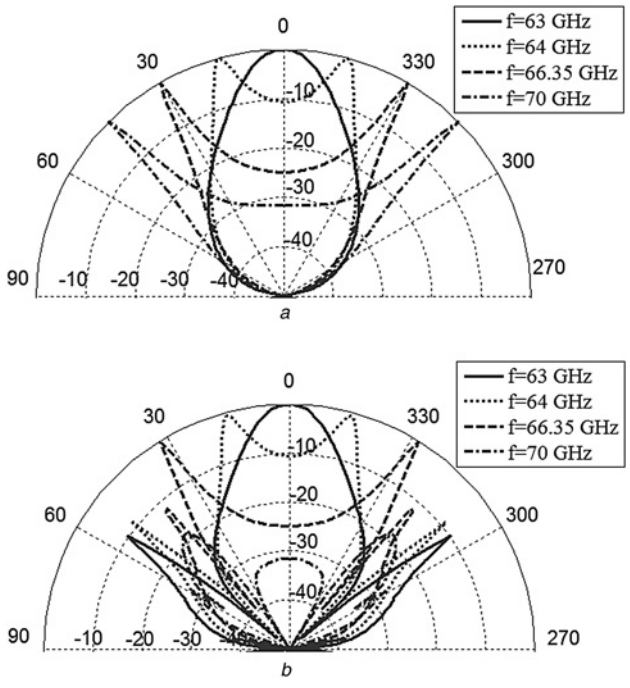

Fig. 11 *Radiation patterns of the LWA for scan angles of $\theta = 0°$, 15°, 30°, 45° that occur at $f = 63$, 64, 66.35, 70 GHz, respectively*

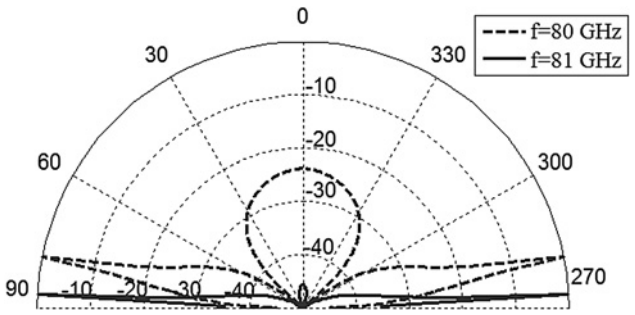

Fig. 12 *H-plane pattern of the LWA for scan angles of $\theta = 79°$, 87° that occur at $f = 80$, 81 GHz, respectively*

by Zhao *et al.* [4] for a Hertzian dipole excitation, it is observed that the radiation pattern is mainly affected by the leaky-wave structure and the source excitation has negligible effect on the pattern as expected.

Fig. 11*b* shows that the E-plane pattern has a side lobe of 10 dB below the main beam. Furthermore, when the scan angle is beyond 40°, the main beam in E-plane is degraded significantly. As mentioned in [4], this degradation of E-plane pattern is due to the TM_0 surface wave that is supported by the grounded dielectric substrate. This surface wave is primarily excited in the E-plane direction. Similar behaviour has been reported for dielectric superstrate LWA in [8]. The H-plane pattern is not affected by this surface wave and the beam can be scanned to near endfire as shown in Fig. 12. In this figure, the beam is scanned to $\theta = 79°$, 87° for $f = 80$, 81 GHz, respectively.

4 Conclusions

Full-wave analysis of a 2D periodic LWA consisting of a 2D periodic array of metallic patches on a grounded dielectric substrate excited by a resonant strip dipole was performed using an elaborate but computationally efficient technique in which the ASM was employed to calculate the Green's function of the periodic structure under aperiodic excitation and MoM was used to calculate the relevant surface current distributions. Finally, the far field of the periodic LWA was calculated using the reciprocity theorem. The input impedance of the source dipole was obtained for different values of dipole width and height in the substrate and the results were compared with those obtained from two commercial EM solvers showing excellent agreement.

Resonant and anti-resonant behaviour of the strip dipole embedded within the 2D periodic structure was demonstrated for the first time and effects of this periodic structure on resonant length of the dipole were investigated. It was also shown that if the dipole is placed at $z_s = h/4$ or $3h/4$ within the substrate, it can achieve a relatively constant near-zero reactance over a fairly large bandwidth. Moreover, it was demonstrated that the Hertzian dipole, which is the only excitation considered in the literature for 2D periodic LWA, is extremely reactive with nearly zero resistance resulting in very low radiation efficiency over the entire operating band of the LWA.

5 References

1 Oliner, A.A., Jackson, D.R.: 'Leaky-wave antennas', in Volakis, J.L. (Ed.): 'Antenna engineering handbook' (McGraw-Hill, New York, 2007, 4th edn.), Ch. 11

2 Zhao, T., Jackson, D.R., Williams, J.T., Oliner, A.A.: 'General formulas for 2-D leaky-wave antennas', *IEEE Trans. Antennas Propag.*, 2005, **53**, (11), pp. 3525–3533

3 Liu, J., Jackson, D.R., Long, Y.: 'Substrate integrated waveguide (SIW) leaky-wave antenna with transverse slots', *IEEE Trans. Antennas Propag.*, 2012, **60**, (1), pp. 20–29

4 Zhao, T., Jackson, D.R., Williams, J.T., Yang, H.Y., Oliner, A.A.: '2-D periodic leaky-wave antennas part I: metal patch design', *IEEE Trans. Antennas Propag.*, 2005, **53**, (11), pp. 3505–3514
5 Zhao, T., Jackson, D.R., Williams, J.T.: '2-D periodic leaky-wave antennas part II: slot design', *IEEE Trans. Antennas Propag.*, 2005, **53**, (11), pp. 3515–3524
6 Burghignoli, P., Lovat, G., Capolino, F., Jackson, D.R., Wilton, D.R.: 'Highly polarized, directive radiation from a Fabry–Pérot cavity leaky-wave antenna based on a metal strip grating', *IEEE Trans. Antennas Propag.*, 2010, **58**, (12), pp. 3873–3883
7 Lovat, G., Burghignoli, P., Capolino, F., Jackson, D.R.: 'Highly-directive planar leaky-wave antennas: a comparison between metamaterial-based and conventional designs'. Proc. European Microwave Association, 2006, vol. 2, pp. 12–21
8 Jackson, D.R., Alexopoulos, N.G.: 'Gain enhancement methods for printed circuit antennas', *IEEE Trans. Antennas Propag.*, 1985, **33**, pp. 976–987
9 Yang, H., Alexopoulos, N.G.: 'Gain enhancement methods for printed circuit antennas through multiple superstrates', *IEEE Trans. Antennas Propag.*, 1987, **35**, (7), pp. 860–863
10 Jackson, D., Oliner, A., Ip, A.: 'Leaky-wave propagation and radiation for a narrow-beam multiple-layer dielectric structure', *IEEE Trans. Antennas Propag.*, 1993, **41**, (3), pp. 344–348
11 Jackson, D.R., Burghignoli, P., Lovat, G., *et al.*: 'The fundamental physics of directive beaming at microwave and optical frequencies and the role of leaky waves', *Proc. IEEE*, 2011, **99**, (10), pp. 1780–1805
12 Lovat, G., Araneo, R., Celozzi, S.: 'Dipole excitation of periodic metallic structures', *IEEE Trans. Antennas Propag.*, 2011, **59**, (6), pp. 2178–2187
13 Bakhtafrouz, A., Borji, A.: 'Application of the array scanning method in periodic structures with large periods', *Electromagnetics*, 2015, **35**, (5), pp. 293–309
14 Rodríguez-Berral, R., Mesa, F., Baccarelli, P., Burghignoli, P.: 'Excitation of a periodic microstrip line by an aperiodic delta-gap source', *IEEE Antennas Wirel. Propag. Lett.*, 2009, **8**, pp. 641–644
15 Araneo, R., Lovat, G., Celozzi, S.: 'Shielding effectiveness of periodic screens against finite high-impedance near-field sources', *IEEE Trans. Electromagn. Compat.*, 2011, **53**, (3), pp. 706–716
16 Rao, S.M., Wilton, D., Glisson, A.W.: 'Electromagnetic scattering by surfaces of arbitrary shape', *IEEE Trans. Antennas Propag.*, 1982, **30**, (3), pp. 409–418
17 Yla-Oijala, P., Taskinen, M.: 'Calculation of CFIE impedance matrix elements with RWG and $\hat{n}\times$ RWG functions', *IEEE Trans. Antennas Propag.*, 2003, **51**, (8), pp. 1837–1846
18 Niciforovic, R.G., Polimeridis, A.G., Mosig, J.R.: 'Fast computation of Sommerfeld integral tails via direct integration based on double exponential-type quadrature formulas', *IEEE Trans. Antennas Propag.*, 2011, **59**, (2), pp. 694–699
19 Koufogiannis, I.D., Polimeridis, A.G., Mattes, M., Mosig, J.R.: 'Real axis integration of Sommerfeld integrals with error estimation'. Sixth European Conf. on Antennas and Propagation (EUCAP), March 2012, pp. 719–723
20 Yuan, M., Sarkar, T.K., Salazar-Palma, M.: 'A direct discrete complex image method from the closed-form Green's functions in multilayered media', *IEEE Trans. Microw. Theory Tech.*, 2006, **54**, (3), pp. 1025–1032
21 Capolino, F., Jackson, D.R., Wilton, D.R., Felsen, L.B.: 'Comparison of methods for calculating the field excited by a dipole near a 2-D periodic material', *IEEE Trans. Antennas Propag.*, 2007, **55**, (6), pp. 1644–1655
22 Volski, V., Vandenbosch, G., Baccarelli, P., *et al.*: 'Interpolation of Green's functions with 2D periodicity in layered media'. Second European Conf. Antennas and Propagation (EuCAP), November 2007, pp. 1–7
23 Michalski, K.A., Mosig, J.R.: 'Multilayered media Green's functions in integral equation formulations', *IEEE Trans. Antennas Propag.*, 1997, **45**, (3), pp. 508–519
24 Valerio, G., Baccarelli, P., Paulotto, S., Frezza, F., Galli, A.: 'Regularization of mixed-potential layered-media Green's functions for efficient interpolation procedures in planar periodic structures', *IEEE Trans. Antennas Propag.*, 2009, **57**, (1), pp. 122–134

6 Appendix

6.1 Calculation of spectral domain Green's functions using transmission line model

The Green's functions of magnetic vector potential and electric scalar potential can be found using spectral domain technique. The transverse transmission line model is shown in Fig. 13. $\tilde{G}_A^{\mathrm{PA}}$ and $\tilde{K}_\varphi^{\mathrm{PA}}$ are

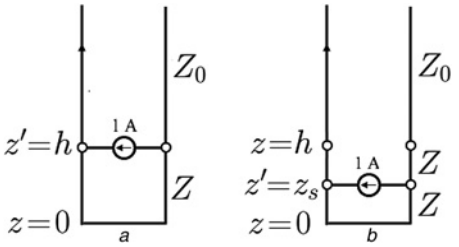

Fig. 13 *Transmission line model of the multilayer structure for*
a $z'=h$
b $z'=z_s$

$$\tilde{G}_A^{\mathrm{PA}} = \tilde{G}_A^{xx,\mathrm{PA}} = \tilde{G}_A^{yy,\mathrm{PA}} = \frac{1}{\mathrm{j}\omega} V_i^{\mathrm{TE}} \tag{26}$$

$$\tilde{K}_\varphi^{\mathrm{PA}} = \frac{1}{k_\rho^2}\left(V_i^{\mathrm{TE}} - V_i^{\mathrm{TM}}\right) \tag{27}$$

V_i is the voltage due to a 1 A parallel current source. From the transmission line analysis, it follows that (see (28))

$$V_i^{\mathrm{TE}}(z=h; z'=z_s) = \frac{1}{\left(Y_0^{\mathrm{TE}} - \mathrm{j}Y^{\mathrm{TE}}\cot(k_z h)\right)} \frac{\sin(k_z z_s)}{\sin(k_z h)} \tag{29}$$

$$V_i^{\mathrm{TE}}(z=h; z'=h) = \frac{1}{\left(Y_0^{\mathrm{TE}} - \mathrm{j}Y^{\mathrm{TE}}\cot(k_z h)\right)} \tag{30}$$

$$V_i^{\mathrm{TE}}(z=h; z'=z_s) = V_i^{\mathrm{TE}}(z=z_s; z'=h) \tag{31}$$

in which

$$Y_0^{\mathrm{TE}} = \frac{k_{z0}}{\omega\mu_0} \tag{32}$$

$$Y^{\mathrm{TE}} = \frac{k_z}{\omega\mu} \tag{33}$$

$$k_{z0} = \sqrt{k_0^2 - k_x^2 - k_y^2} \tag{34}$$

$$k_z = \sqrt{k^2 - k_x^2 - k_y^2} \tag{35}$$

Similar equations can be derived for V_i^{TM} by replacing TE by TM in above equations and using

$$Y_0^{\mathrm{TM}} = \frac{\omega\varepsilon_0}{k_{z0}} \tag{36}$$

$$Y^{\mathrm{TM}} = \frac{\omega\varepsilon}{k_z} \tag{37}$$

$$V_i^{\mathrm{TE}}(z=z_s; z'=z_s) = \frac{1}{Y^{\mathrm{TE}}.\begin{pmatrix} \left[\left\{Y_0^{\mathrm{TE}} + \mathrm{j}Y^{\mathrm{TE}}\tan\left(k_z(h-z_s)\right)\right\}/\left\{Y^{\mathrm{TE}} + \mathrm{j}Y_0^{\mathrm{TE}}\tan\left(k_z(h-z_s)\right)\right\}\right] \\ -\mathrm{j}\cot(k_z z_s) \end{pmatrix}} \tag{28}$$